Electronic Supplementary Material (ESI) for Nanoscale.

Supporting Information: How do interfaces alter the dynamics of supercooled water?

Piero Gasparotto,*,† Martin Fitzner,‡ Stephen J. Cox,¶ Gabriele Cesare Sosso,§ and Angelos Michaelides*,¶

†*Scientific Computing Division, Paul Scherrer Institute, 5232 Villigen, Switzerland*

‡*Thomas Young Centre, London Centre for Nanotechnology and Department of Physics and Astronomy, University College London, London WC1E 6BT, UK*

¶*Yusuf Hamied Department of Chemistry, University of Cambridge, Lensfield Road, Cambridge CB2 1EW, United Kingdom*

§*Department of Chemistry, University of Warwick, Gibbet Hill Road, Coventry CV4 7AL, United Kingdom*

E-mail: piero.gasparotto@psi.ch; am452@cam.ac.uk

S1: Equilibration workflow

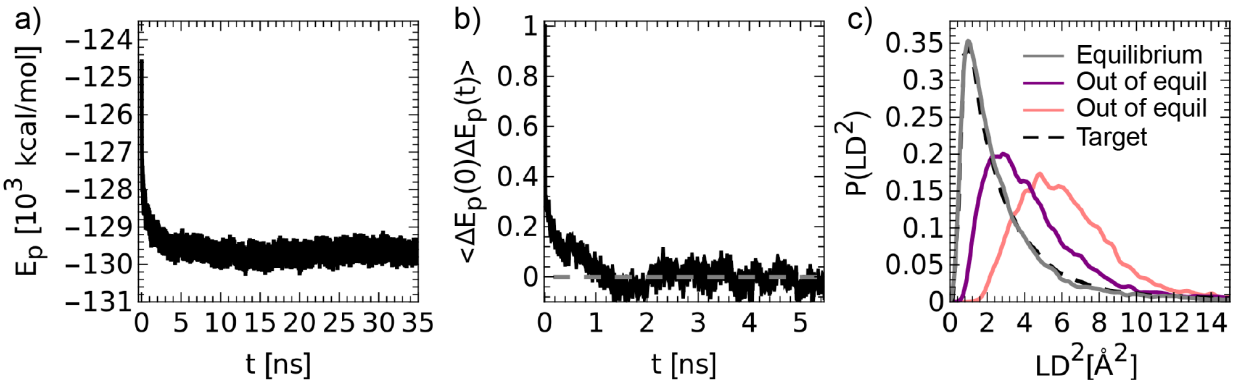

Figure 1: a) Evolution of the potential energy for a 12 nm-thick slab at 230K equilibrated in the NVT ensemble for 35 ns. The trend becomes constant around 20 ns which is the time needed to relax the slab starting from a bulk configuration sampled from a trajectory at equilibrium. b) Autocorrelation function (ACF) of the potential energy from the last 15 ns plotted in a. The decay of the ACF is in the order of few ns. c) LD distributions for samples from the trajectory described in a). The black dashed line represents the target LD ditribution for the 12 nm-thick slab at 230 K. This was computed from 15 snapshots drawn from a well-equilibrated trajectory. Checking for the convergence of the LD distribution is an effective way to test for the proper equilibration of the slabs, since monitoring the potential energy only could be misleading when studying DH in water.

For each bulk system we start from a (cubic) simulation box of the desired size at the target experimental density. We then perform an initial NPT equilibration of 10 ns at the target temperature, setting the pressure to 0 atm. We discard the first 6 ns and use the last 4 ns to compute the average volume and fix the cell size to be used in any future NVT simulations. A further run of 35 ns in the NVT ensemble starting from the last snapshot of the NPT equilibration is eventually performed. For bulk systems, this run equilibrates relatively rapidly and one can safely discard only the first 5 ns of the trajectory and use the remaining 30 ns as the production run from which to extract the samples for the ISOCA. The same workflow applies to droplets. Slabs are instead prepared starting from an already equilibrated bulk by replicating the cell along the z direction up to desired size. All the slabs presented in this work have a later cell length of ∼4.5 nm (size varies according temperature). We carefully tested two slab simulation setups:

- fully periodic box with a large vacuum region (5 times the slab thickness, as in ref. 1) in the direction perpendicular to the interface (`periodic p p p` command)
- LAMMPS slab setup, with periodicity applied only to directions parallel to the slab plane (`periodic p p f` and `kspace_modify slab volfactor` commands[2]). This effectively tells LAMMPS to treat the system as if it was non-periodic in z by automatically inserting empty volume between slab's replicas and removing dipole inter-slab interactions so that slab-slab self-interaction is effectively off. The `volfactor` is set to 3.0 which is the recommended value and corresponds to the ratio of the extended dimension in z divided by the slab thickness.

Both of these simulation approaches lead to the same results. In general we notice that the equilibration of slabs tends to be slower than that of bulk and droplets. Fig. 1a shows the time evolution of the potential energy over 35 ns for a 12 nm-thick slab (27648 atoms) at 230 K in the NVT ensemble. One can notice how the potential energy becomes constant around 18 ns, which makes challenging the equilibration of large slabs at high supercooling. It is non trivial to know *a priori* what could be the minimum trajectory length needed to collect enough statistics to characterise properly the DH. To address this issue, we used the last well-equilibrated 15 ns of the trajectory to compute the auto-correlation function (ACF) of the potential energy (fig. 1b), which provides an estimate of the sampling efficiency of our simulations. Computing ACFs from MD simulations is far from trivial and obtaining the exact auto-correlation time from the integral of the ACF was not part of the scope of this study. However, even if the resulting ACF is noisy due to the relatively short time series used, it can still be used to infer qualitatively its decay to zero, which happens in a time of the order of few nanoseconds (several time larger than τ_0). This corresponds to the minimum time (Δt) required to sample two consecutive uncorrelated samples from the trajectory. A reasonable choice is to set Δt=$4t_0$, which at 230K corresponds to $\sim$2.5 ns. This means that to generate 30 configurations to be use in the ISOCA (necessary to converge the LD), we need a trajectory long at least 75 ns (beyond the initial 18 ns equilibration). Given

the time scales and slab sizes considered in this study, we opted to perform most of the simulations involving larger systems at T=250 K only, a temperature at which the DH is still present, but the dynamics is ∼20 times faster (Δt∼0.1 ns) than T=230 K. Finally, to verify the proper equilibration of the dynamical properties we also monitored the shape of the LD distributions for each configuration (fig. 1c). Indeed, when the configuration used in the ISOCA comes from a part of the trajectory that is not yet fully equilibrated, its LD distribution deviates considerably from the target distribution.

S2: The Role of Statistics in the calculation of LD

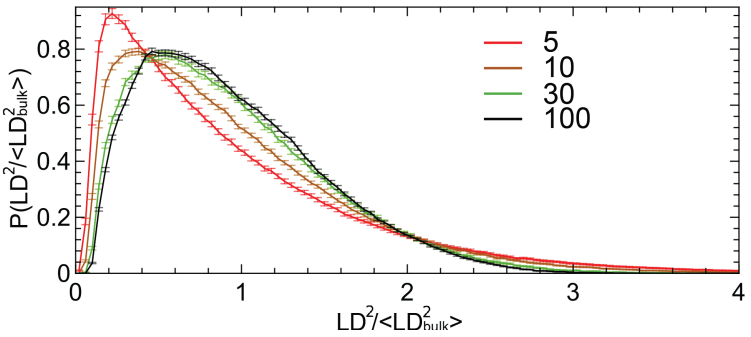

Figure 2: a) Bias in the calculation of LD as a function of the number of runs used in ICA. The error bars correspond to the standard error of the mean associated to the mean LD estimated from 400 bootstrap resamples. Convergence is reached for N=30. Different number of independent initial independent frames are use. ISOCA shown in the main text is done using 40 runs.

ISOCA[3,4] allows to estimate the local diffusivity of water molecules, which is useful to quantify the DH in water. ISOCA consists in starting N trajectories from the same initial configuration, by setting randomly the velocities of each atom and evolving the dynamics in the NVE ensemble up to the time of maximum heteregoneity (t_0, see ref. 5 for a proper definition). To test the minimum number of trajectories N to be used in our ICA, we tested how the LD distribution of a single snapshot converges as a function of N, for liquid bulk water at 230 K. As shown in Fig. 2a, good convergence of the LD distribution is obtained already for N =30, which makes computationally affordable the exploration of DH in large

systems. The quality of ISOCA largely depends on not only the number of independent runs but also the number of starting configurations used for the analysis. As a rule of thumb, we find that a minimum of 15 independent snapshots is enough to collect a good estimate of LD profiles. To converge the LD distribution fewer snapshots are needed and around 10 independent snapshots could be enough. However, we typically collect between 30 and 50 independent snapshots.

S3: Role of MM and MI definitions

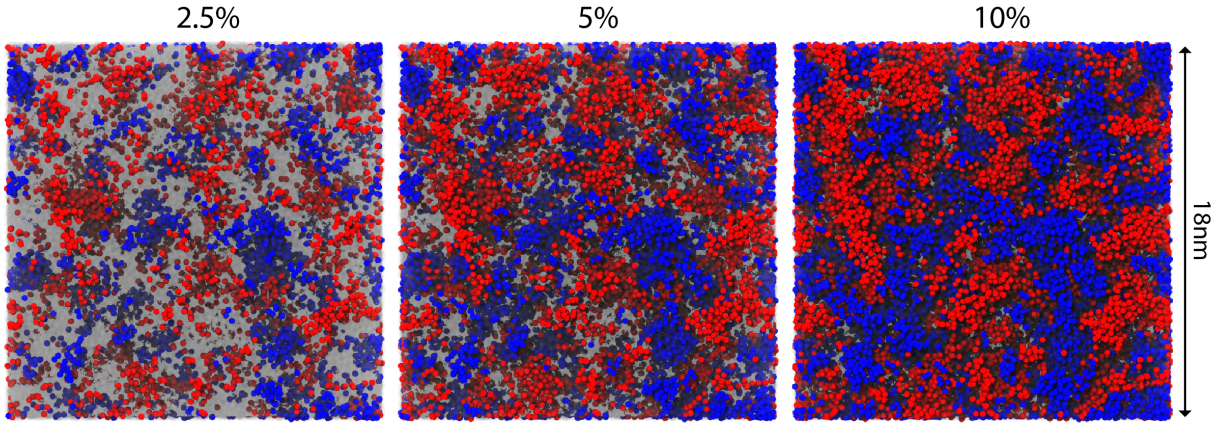

Figure 3: Snapshot from an NVT simulation of liquid bulk water at 230K. From left to right we use an increasing top and bottom percentiles of the LD distribution to define MM (red) and MI (blue) species. The snapshots are from a simulation box containing ∼200000 molecules and LD values are computed using ISOCA with N=30.

Following the suggestion from ref. 5 we define MM and MI according to the top (MM, red) and bottom (MI, blue) 5 percentiles of the LD probability distribution of the bulk. In fig. 3 a snapshot from a liquid bulk at 230K is shown with oxygens coloured according to different different definitions of MM and MI. This is in line with the results of Sciortino et al.,[6] where the fraction of MM molecules is found to be ∼6–7%. Setting the thresholds to different percentiles affects mainly the domains' size, but does not change the qualitative interpretation of the results. Indeed the segregation of molecules into different dynamical domains is always evident and the relative spatial distributions of the domains is consistent

between the different definitions.

S4: DH cluster size and comparison of with previous works

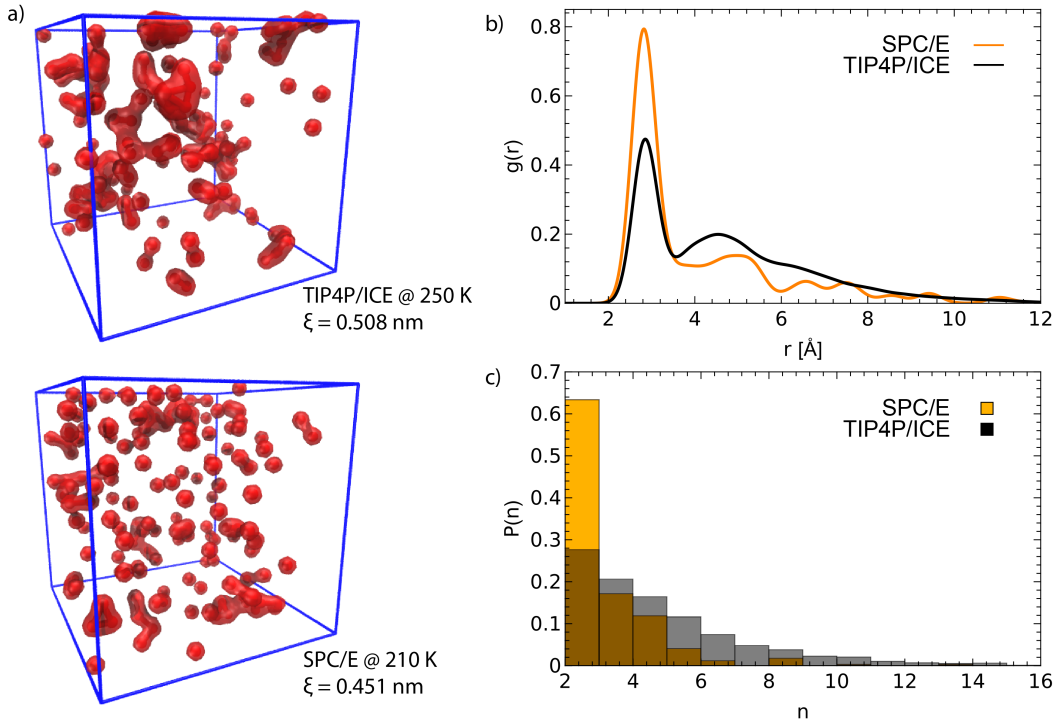

Figure 4: a) ISOCA analysis applied to supercooled TIP4P/Ice at 250 K compared to SPC/E water at 210 K (both at 1 atm). At these temperatures the two water models have a comparable τ_0, i.e. 27 ps for TIP4P/Ice and 28.75 ps for SPC/E. The snapshots are from bulk NVT simulations equilibrated at ambient pressure. The box length is 45.231 Åfor SPC/E and 45.5,Å for TIP4P/Ice. The red isocontours represent the extent of the MM-clusters and the corresponding ξ correlation length as introduced in ref. 7. b) The pair connectivity function $g(r)$ for the two water models respectively. c) Distribution of MM-cluster sizes, showing that TIP4P/Ice tends, on average, to form larger dynamical clusters than SPC/E as shown in panel a).

Dynamical heterogeneity in bulk liquid water has been studied extensively in the literature. To probe DH we use here iso-configurational analysis, which was originally developed to see the connection between static and dynamic heterogeneities in deeply supercooled glass-formers. We find that the clusters of MM and MI identified using ISOCA are on the length

scale of a few nanometers, in line with previous work on DH in bulk water.

To validate the ability of ISOCA in capturing DH in water, we have checked our approach against previous results obtained for SPC/E water.[8] DH in SPC/E water has been widely studied in the past, showing good agreement with experiments.[7,9–12] When comparing SPC/E with TIP4P/Ice one should consider the fact that the melting point of SPC/E is 215 K, while that of TIP4P/Ice is 272.2 K.[13] We performed a grid search on SPC/E and found that at 210 K τ_0=28.75 ps, which is comparable to that of TIP4P/Ice at 250 K. Fig. 4a and b shows the results of ISOCA applied to two bulk liquids respectively, showing a strong similarity of the spatial extent of DH domains. Giovanbattista et al.[7] reported that the dynamical correlation length ξ for the MM clusters is about 6 Å around 200 K for SPC/E bulk water. Their analysis was previously used to study DH of binary LJ systems and is based on the self-part of the time-dependent van Hove correlation function[14] and the non-Gaussian parameter $\alpha_2(t)$ as defined in ref. 6. From the maximum of $\alpha_2(t)$ a characteristic time t^* is derived, which is used to identify the fraction of MM molecules (which, in line with our definition, correspond to the ∼6-8% fraction). Here we show that our methodology is consistent with the approach proposed by Giovanbattista and co-workers and show that labelling molecules using ISOCA leads to comparable results. Following their recipe, we define MM-clusters as those mobile molecules whose nearest-neighbor oxygen-oxygen is less than 0.315 nm, the first minimum of the oxygen-oxygen radial distribution function in SPC/E bulk water. To characterize the morphology of the clusters by estimating the geometric size, we define the correlation length ξ as:

$$\xi^2 = \frac{\int r^2 g(r) dr}{\int g(r) dr} ,$$

where $g(r)$ is the correlation function or pair connectivity[15] defined as the probability that two molecules belonging to the same MM-cluster are separated by a distance r. ξ can be interpreted as the average root-mean-square distance between two molecules in a cluster and is thus comparable with the square root of the LD distribution's first moment. As shown in Fig. 4, we find that ξ in TIP4P/Ice and SPC/E are comparable and in line with the results

of Giovanbattista et al.

Similarly, Shi et al.[16] reported a structural length 6Å at 230 K for TIP5P.[16] In contrast to Giovanbattista et al., Shi and coworkers described the spatial correlation of DH in water from the fourth-order time-dependent density correlation function $g_4(r)$ following the approach introduced in ref. 17. Then, the dynamic correlation length ξ_4 can be extracted by an envelope fit of $g_4(r)$ to an exponential function (discarding the first two peaks). The lengths found with this approach are in line with the typical correlation length emerging from the ISOCA analysis. This is not surprising and indeed in a previous work[18] Shi and coworkers[18] investigated the trend of ξ_4 as a function of temperature for TIP5P water at 1 bar. They found that ξ_4 reaches a maximum of $\sim$6 Å corresponding to two molecular sizes, in agreement with χ_4 maximum at the same temperature. Since τ_0 is the time at which χ_4 has its maximum, this confirms the analogy between ξ_4 and the square root of the average LD value derived from ICA. Furthermore, all these results are in line with the short structural correlation lengths of $\sim$4 Å recently reported by femtosecond x-ray experiment.[19]

S5: Dynamical and structural surface decay lengths

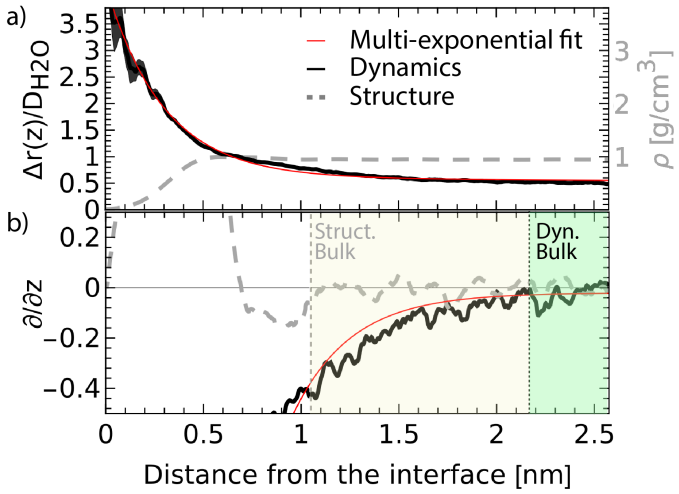

Figure 5: Decay of structural and dynamical profiles at the standard mean surface. a) The median LD (black line) and the mean density (gray dashed line) profiles are shown. A multi exponential fit (red line) is necessary to fit the decay of LD at the surface. b) First derivatives of the corresponding functions shown in panel a. The derivative of the mean structural profile gets to zero at ∼1 nm from the interface, while dynamics recover bulk at ∼2.2 nm.

Fig. 5b gives a quantitative estimation of distances from the standard interface at which the liquid's structure and dynamics recover their bulk values, respectively. It's clear the structural bulk starts at ∼1 nm from the surface, as the mean profile's derivative goes to zero for such distance from the interface. Different is the case for dynamics, where the same analysis show that a molecule can be considered in a bulk-like environment only for distances larger than 2.2 nm.

S6: Effect of box size and shape

Recently Longford et al.[20] studied the vapour/liquid interface of water and LJ systems. The found that increasing the size of interfacial systems may not always lead to ensemble average properties that possess low uncertainty. This is due to a finite size effect affecting interfacial molecular simulations that is proportional to the width-to-surface-area. In their

study they showed that increasing the number of particles in the simulation by increasing the film thickness without a subsequent increase in the surface area (lateral box size) affects the estimate of the surface tension (not the expectation values, only its variance). In our work the focus is not about estimating the liquid/vapour surface tension, however we carefully checked that the highly asymmetric cell shape used does not induce any artefact in the estimation of LD. Fig. 6b shows the comparison of LD distributions for bulk water at 230 K (and 1 bar) computed from boxes of different sizes and shapes. A similar test for free standing films is shown in fig. 6a, where the LD distributions are computed from simulation boxes of different lateral size. These results confirm that different sizes and shapes does not introduce any artefacts in the results.

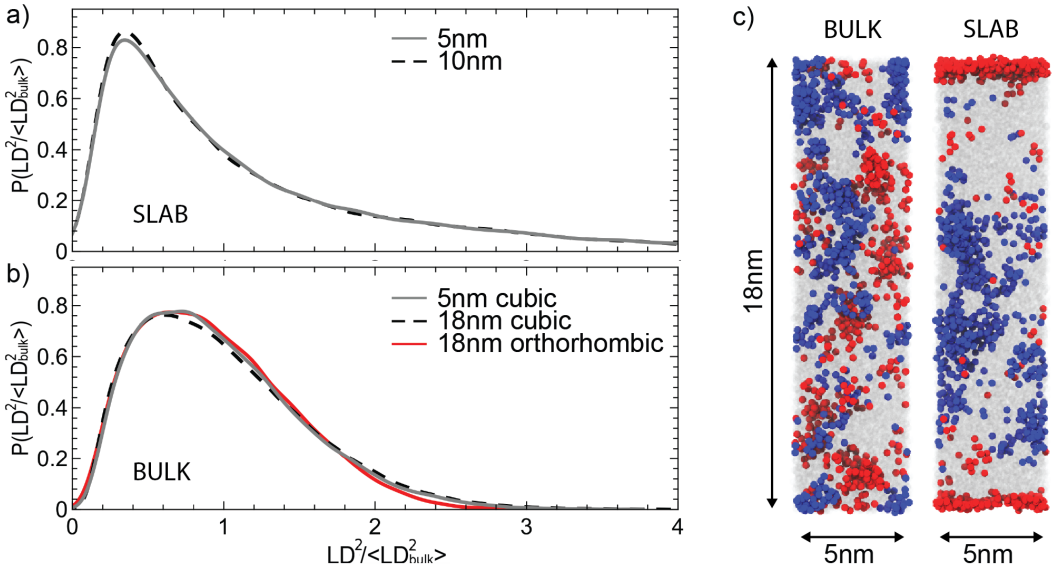

Figure 6: a) LD distribution for a 5 nm-thick slab computed from simulations with different lateral box sizes. 5 nm is enough to converge the LD distribution in the slab geometry. b) Convergence of the LD distribution in bulk as a function of the box shape and size. Using a cubic box of length 5 nm is enough to obtain the same results computed from a much larger bulk (18 nm^3 cubic cell). The anisotropy of the cell has no effect on the LD distribution as shown by the red curve, which was computed from a 5 nm x5 nm x18 nm simulation box. c) Snapshots from of a slab and a bulk simulations with cells of identical shape (5 nm x5 nm x18 nm). The shape of the box has no influence on the dynamical domains in both the bulk and the slab, and is not responsible for the peculiar dynamical effects observed in the slab's centre.

S7: Effect of slab's thickness on dynamical fluctuations

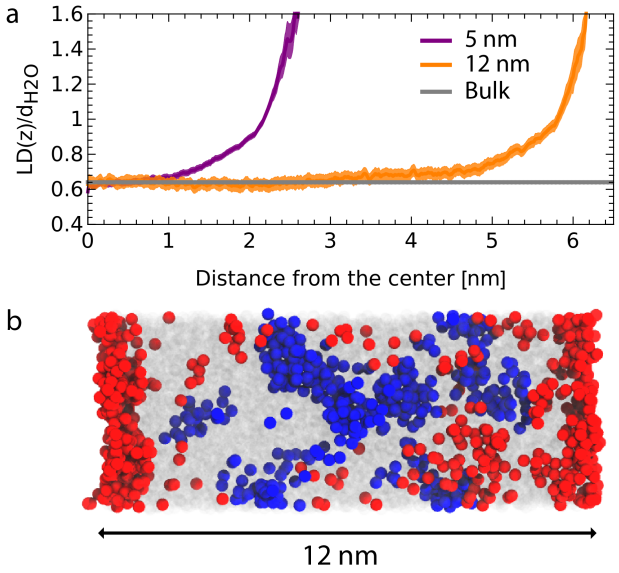

Figure 7: a) Comparison between the median LD(z) profiles of 5 nm- (purple) and 12 nm- (orange) thick free-standing films at 250K. The NVT equilibration for the new 12 nm film was 10ns and the ISOCA was performed on 10 independent snapshots sampled from the equilibrated NVT trajectory. b) Snapshot for the 12 nm-thick film at 250 K. Only the oxygens are shown, with MM molecules coloured in red and MI in blue. It's clear how large dynamical clusters are still present and well-distinct also for the 12 nm film.

Chen et al.[21] studied the transport behaviour of water molecules inside a model carbon nanotube for the TIP3P water model[22] at 298 K. They found that the nominal viscosity of the confined liquid is a function of the tube size and is strongly dependent on the flow rate, which is directly related to the shearing stress between the liquid molecules and the solid atoms. Comparing our results with those of Chen et al. is not trivial, as in our framework we only have access to a static picture that allows linking local structure and local dynamics at a fixed point in time. However, even though studying the link between transport phenomena and DH is not the scope of this study, we believe that exploring the dependence between DH and the confinement size in free-standing slabs is an interesting point. For this reason, we report in Fig. 7a comparison between the LD(z) profile of the 5 nm-thick slab discussed in the main text, with that of a 12 nm-thick slab. We found that they both converge to bulk at their center and that DH is still clearly visible across all the 12 nm film, with well-separated

mobile and immobile domains.

S8: Comparing local dynamics with local structure

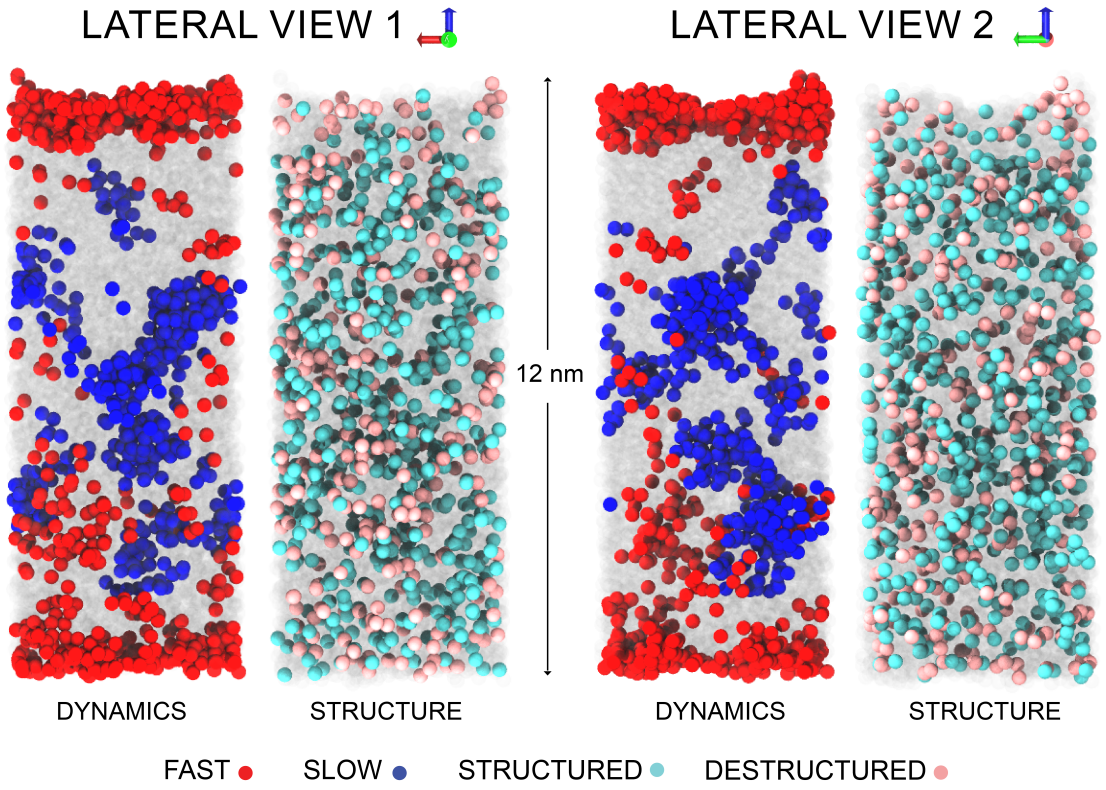

Figure 8: Different lateral views for local dynamics and structure in a 12 nm-thick TIP4P/ICE water film at 250 K and 0 atm. On the left, the local dynamics is shown by coloring oxygen atoms according to the top and bottom 5 percentiles of the LD distribution. On the right, the local structure is shown by coloring oxygen atoms according to the top and bottom 5 percentiles of the distribution of the LSI structural descriptor. The LSI aims at measuring the extent of the gap between the first and the second hydration shells surrounding a water molecule.[23] The LSI thus focuses on the translational order and probes the local structure beyond the first hydration shell.[24] It has been especially used to study the structure of supercooled water.[25] One can see how DH is present in TIP4P/ICE water at 250 K, and how LD is a powerful tool to capture it and visualize it with atomic resolution.

LD quantifies the propensity of each molecule to displace in the local surrounding within the time of maximum heterogeneity (t_0, characteristic time to probe DH given a specific thermodynamical state[5]). This is precisely what allows us to visualise DH at the atomic

level and link it with local structural properties. Throughout the paper, we used the median LD(z) profile to visualize how on average perturbs local dynamics (and local structure, when considering the density) as a function of the distance from the surface. However, one can visualize the heterogeneous nature of DH in space by colouring directly each molecule in each configuration. Fig. 8 shows different lateral views for a single snapshot in time of a 12 nm-thick slab coloured according the local dynamical descriptor used here (LD) and a local structural descriptor (Local Structure Index (LSI)[23,24]). Fig. 8 shows clearly how LD is a dynamical descriptor able to capture well the heterogeneous nature of dynamics in supercooled water, and confirms the argument that the dynamical heterogeneity does not trivially reflects into a local structure counterpart.

S9: Effect of the thermostat on the DH

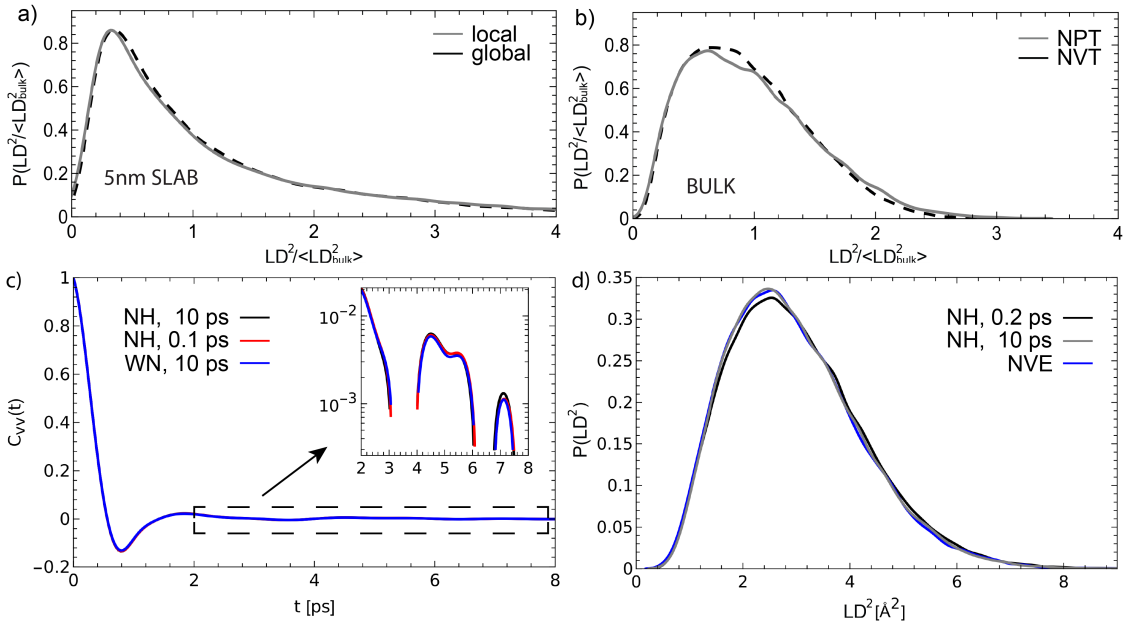

Figure 9: a) Convergence of the LD distribution for a 5 nm-thick slab at 230K using different thermostats. The black dashed line represents a Nosé-Hoover Chain (with a coupling constant of 0.2 ps) and is computed using ISOCA from 18 snapshots with N=160, while the gray line represents white noise Langevin (with a coupling constant of 10 ps) and is computed from 18 snapshots using N=100. b) Convergence of the LD distribution of liquid water in bulk at 230 K using a box of 3072 molecules. The gray line represents the NPT ensemble and is obtained using ISOCA on 7 snapshots with N=50. The black line represents the NVT ensemble and is obtained using ISOCA on 20 independent snapshots and N=150. c) Velocity autocorrelation funtion for different thermostats and coupling constants computed from a 200 ps NVT trajectory at 250 K. The choice of the thermostats and of the coupling constant does not affect the dynamics of supercooled water. The inset shows a semi-log plot of the tail, to show that the only difference between the functions comes from statistical noise. d) Non-normalized LD distributions for bulk water at 250 K, computed with ISOCA applied to the same systems, but using different thermostatting strategies in the ISOCA runs. The thermostat has minimal effects on the DH and is not responsible for the long range dynamical correlations discussed for the slabs in the main text.

We tested the possibility of observing artefacts induced by the use of different thermostats and thermodynamic ensembles. No temperature gradients are observed in slab simulations when using both global (e.g. Nosé-Hoover Chain) and local thermostats (e.g. White Noise Langevin). Fig. 9a shows how the same LD distribution in a 5 nm-thick slab at 230 K can be obtained equilibrating the trajectory with two different thermostats. Furthermore, the

equilibrium LD distributions appears to be the same also when using different thermodynamic ensembles. Fig. 9b shows results for ISOCA performed starting from the NPT (gray) (at 1 bar) and NVT (black) ensembles at 230K. The NPT distribution is noisier due to the smaller number of samples used (four independent snaphots of 3072 water molecules). Fig. 9d and c show a careful analysis of the effect of the coupling constant of the thermostat on DH. We find that both the velocity-velocity autocorrelation function and the LD distribution are not affected by the choice of the coupling constant of the thermostat.

References

(1) Haji-Akbari, A.; Debenedetti, P. G. Computational investigation of surface freezing in a molecular model of water. *Proceedings of the National Academy of Sciences* **2017**, *114*, 3316–3321.

(2) Yeh, I.-C.; Berkowitz, M. L. Ewald summation for systems with slab geometry. *The Journal of chemical physics* **1999**, *111*, 3155–3162.

(3) Widmer-Cooper, A.; Harrowell, P. On the study of collective dynamics in supercooled liquids through the statistics of the isoconfigurational ensemble. *The Journal of Chemical Physics* **2007**, *126*, 154503.

(4) Sosso, G. C.; Colombo, J.; Behler, J.; Del Gado, E.; Bernasconi, M. Dynamical heterogeneity in the supercooled liquid state of the phase change material GeTe. *The Journal of Physical Chemistry B* **2014**, *118*, 13621–13628.

(5) Fitzner, M.; Sosso, G. C.; Cox, S. J.; Michaelides, A. Ice is born in low-mobility regions of supercooled liquid water. *Proceedings of the National Academy of Sciences* **2019**, *116*, 2009–2014.

(6) Sciortino, F.; Gallo, P.; Tartaglia, P.; Chen, S.-H. Supercooled water and the kinetic glass transition. *Physical Review E* **1996**, *54*, 6331.

(7) Giovambattista, N.; Buldyrev, S. V.; Stanley, H. E.; Starr, F. W. Clusters of mobile molecules in supercooled water. *Physical Review E* **2005**, *72*, 011202.

(8) Berendsen, H.; Grigera, J.; Straatsma, T. The missing term in effective pair potentials. *Journal of Physical Chemistry* **1987**, *91*, 6269–6271.

(9) Scala, A.; Starr, F. W.; La Nave, E.; Sciortino, F.; Stanley, H. E. Configurational entropy and diffusivity of supercooled water. *Nature* **2000**, *406*, 166–169.

(10) Starr, F. W.; Angell, C. A.; La Nave, E.; Sastry, S.; Scala, A.; Sciortino, F.; Stanley, H. E. Recent results on the connection between thermodynamics and dynamics in supercooled water. *Biophysical chemistry* **2003**, *105*, 573–583.

(11) Giovambattista, N.; Buldyrev, S. V.; Starr, F. W.; Stanley, H. E. Connection between Adam-Gibbs theory and spatially heterogeneous dynamics. *Physical review letters* **2003**, *90*, 085506.

(12) Giovambattista, N.; Mazza, M. G.; Buldyrev, S. V.; Starr, F. W.; Stanley, H. E. Dynamic heterogeneities in supercooled water. *The Journal of Physical Chemistry B* **2004**, *108*, 6655–6662.

(13) Abascal, J.; Sanz, E.; García Fernández, R.; Vega, C. A potential model for the study of ices and amorphous water: TIP4P/Ice. *The Journal of chemical physics* **2005**, *122*, 234511.

(14) Hansen, J.-P.; McDonald, I. R. *Theory of simple liquids*; Elsevier, 1990.

(15) Stauffer, D.; Aharony, A. *Introduction to percolation theory*; CRC press, 2018.

(16) Shi, R.; Russo, J.; Tanaka, H. Common microscopic structural origin for water's thermodynamic and dynamic anomalies. *The Journal of chemical physics* **2018**, *149*, 224502.

(17) Lačević, N.; Starr, F. W.; Schrøder, T.; Novikov, V.; Glotzer, S. Growing correlation length on cooling below the onset of caging in a simulated glass-forming liquid. *Physical Review E* **2002**, *66*, 030101.

(18) Shi, R.; Russo, J.; Tanaka, H. Origin of the emergent fragile-to-strong transition in supercooled water. *Proceedings of the National Academy of Sciences* **2018**, *115*, 9444–9449.

(19) Kim, K. H.; Späh, A.; Pathak, H.; Perakis, F.; Mariedahl, D.; Amann-Winkel, K.; Sellberg, J. A.; Lee, J. H.; Kim, S.; Park, J.; Nam, K. H.; Katayama, T.; Nilsson, A. Maxima in the thermodynamic response and correlation functions of deeply supercooled water. *Science* **2017**, *358*, 1589–1593.

(20) Longford, F. G.; Essex, J. W.; Skylaris, C.-K.; Frey, J. G. Unexpected finite size effects in interfacial systems: Why bigger is not always better—Increase in uncertainty of surface tension with bulk phase width. *The Journal of Chemical Physics* **2018**, *148*, 214704.

(21) Chen, X.; Cao, G.; Han, A.; Punyamurtula, V. K.; Liu, L.; Culligan, P. J.; Kim, T.; Qiao, Y. Nanoscale fluid transport: size and rate effects. *Nano letters* **2008**, *8*, 2988–2992.

(22) Jorgensen, W. L.; Chandrasekhar, J.; Madura, J. D.; Impey, R. W.; Klein, M. L. Comparison of simple potential functions for simulating liquid water. *The Journal of chemical physics* **1983**, *79*, 926–935.

(23) Shiratani, E.; Sasai, M. Growth and collapse of structural patterns in the hydrogen bond network in liquid water. *The Journal of chemical physics* **1996**, *104*, 7671–7680.

(24) Duboué-Dijon, E.; Laage, D. Characterization of the local structure in liquid water by various order parameters. *The Journal of Physical Chemistry B* **2015**, *119*, 8406–8418.

(25) Shiratani, E.; Sasai, M. Molecular scale precursor of the liquid–liquid phase transition of water. *The Journal of chemical physics* **1998**, *108*, 3264–3276.